Visual Tracking in Wind with Field of View Constraints

Jeffery Saunders[*], Randal W. Beard[†]

July 27, 2011

Abstract

This paper addresses the problem of tracking a ground-based target with a fixed camera pointing out the wing of a micro air vehicle that is subjected to constant wind. Rather than planning explicit trajectories for the vehicle, a nonlinear image-based feedback guidance strategy is developed that maintains the target in the field-of-view of the camera. We show that under ideal conditions, forcing the target to the center of the image results in flight paths that are elliptical trajectories. We also show that if the target is allowed to move in the image plane, circular orbits are possible. Both simulation and flight tests are used to demonstrate the effectiveness of the proposed algorithm and its robustness to wind gusts.

Nomenclature

Mathematical symbols are listed in the order that they are used in the document.

ρ	Range to target
η	Bearing to target
V_a	Airspeed
V_w	Wind speed
ψ	Heading angle of aircraft
χ_w	Wind direction
g	Gravitational constant (9.8 m/s)
ϕ	Roll angle
α_e	Elevation angle of optical axis
$\bar{\eta}$	Bearing limit imposed by field-of-view constraint
h	Altitude
$\bar{\phi}$	Roll angle limit imposed by field-of-view constraint
φ	Deviation of optimal axis from line of sight vector

[*]Raytheon Missile Systems, Tucson, Arizona

[†]Electrical and Computer Engineering, Brigham Young University, Provo, Utah. Corresponding author. Email: beard@byu.edu

$\bar{\varphi}$ Longitudinal field-of-view limit of camera
t Time
ϕ_{up} Algorithmic upper limit on roll angle
ϕ_{low} Algorithmic lower limit on roll angle
ϕ^- Unconstrained roll angle that maintains field-of-view constraint
θ A selectable gain between zero and one
ϕ^c Commanded roll angle
ν Slack variable used to minimize stand-off distance
k Positive control gain
S_η Set of bearing angles within the field-of-view
T Sample rate

1 Introduction

This paper focuses on autonomous vision-based *target tracking*, defined here as maintaining a target in the field-of-view of an onboard strap-down camera. Target tracking is an enabling technology for a wide range of potential military and civilian uses of small and miniature fixed wing air vehicles (referred to hereafter as MAVs). Vision-based target tracking is challenging, in part because the motion of the target and/or gusts of wind may cause the target to move outside the field of view of the camera. Therefore a guidance algorithm that guarantees that the target remains in the field of view is highly desirable.

Vision-based target tracking with fixed wing vehicles has been addressed in the literature. For example, Thomasson develops an open-loop approach to target tracking in wind [13] by assuming an elevation controlled (single axis gimbal) camera and constant wind. He shows that the air vehicle must fly an ellipse with the target located at one of its foci and with the major axis of the ellipse aligned perpendicular to the direction of the wind. The calculation of the dimensions of the ellipse is based on prior knowledge of the magnitude and direction of the wind velocity. Given the kinematic constraints of the MAV, the wind velocity, and the target velocity, an elliptical trajectory is generated for the MAV to track. If the wind velocity and target velocity remain constant, the MAV will track the target indefinitely, but since the method is open-loop, it will not be robust to changes in wind, gusts, or target motion. This paper improves on [13] by using a feedback guidance strategy without path planning that still results in elliptical orbits around the target. In addition, we remove the requirement for a single axis gimbal.

Successful path planning solutions to target tracking problems have been demonstrated in [2, 3, 4, 7, 8, 10, 11, 12]. The general approach is to estimate the position of the MAV, the position of the target and the wind, based on current measurements, and to use the current estimate to regenerate an open-loop trajectory. Reference [3] generates paths to a landing position based on vision of a runway or other landmark. Moving targets are tracked using dynamic planning in [2, 4, 7, 8, 11, 12] where gimbaled cameras are used to help track the

targets. Unfortunately, gimbals are not always feasible on MAVs. Removing the gimbal introduces additional kinematic constraints and path planning becomes more difficult. Additionally, a gust of wind or a sudden change in the course of the target may push it outside the field-of-view before a response is generated, possibly causing the MAV to lose the target altogether. This paper differs from previous work by using image-based feedback to maneuver the MAV so that the target remains in the camera field-of-view.

A feedback control law is developed in [14] for target tracking from kinematic laws, where it is assumed that the target velocity is known, that there is no wind, and that the camera is gimbaled. The flight paths in [14] are circular trajectories centered around the target. Circular, rather than elliptical trajectories are possible because of the degree of freedom provided by the gimbal. However, the gimbal adds weight and may not be feasible on small MAVs. We build on these results by developing a feedback law around the image plane and by removing the gimbal.

An adaptive feedback approach to target tracking using computer vision is developed in [5, 6]. A fixed angle camera is used to track a target and an adaptive scheme estimates the target velocity and other parameters. Adaptive control however often suffers from transients that affect initial flight performance in hardware tests.

In this paper a non-linear guidance law is developed using range-to-target and bearing-to-target information obtained from target motion in the image plane. This approach reacts to target motion in the image plane by maneuvering the aircraft to "push" the target toward the center of the camera field-of-view. The resulting trajectory is an elliptical orbit, where the eccentricity of the ellipse is a direct function of the strength of the wind. We note that constant target motion and constant ambient wind have the same effect on the relative dynamics. Therefore, for simplicity and without loss of generality, in this paper we will assume a stationary target and a constant ambient wind. The goal is to maintain the target in the camera field-of-view in the presence of wind. In this paper we do not address the image processing algorithms that are required to obtain range and bearing information from the video sequence. For an example of an algorithm that uses vision data to construct range and bearing, the reader is referred to [15]. Since the focus of this paper is on the guidance algorithm, we make the (admittedly unrealistic) assumption that noiseless and non-delayed vision data is available at 30 frames per second. Noisy and delayed measurements will add an additional source of error that will be studied in future work.

2 System Dynamics and Problem Description

2.1 Relative dynamics

The MAV is assumed to have an autopilot with inner control loops to command roll angle. We will assume that the autopilot maintains a constant commanded altitude and airspeed. The relative dynamics between the MAV and the target

are best described by polar coordinates in the MAV body frame as shown in Figure 1. Let ρ be the range-to-target and let η be the bearing-to-target as

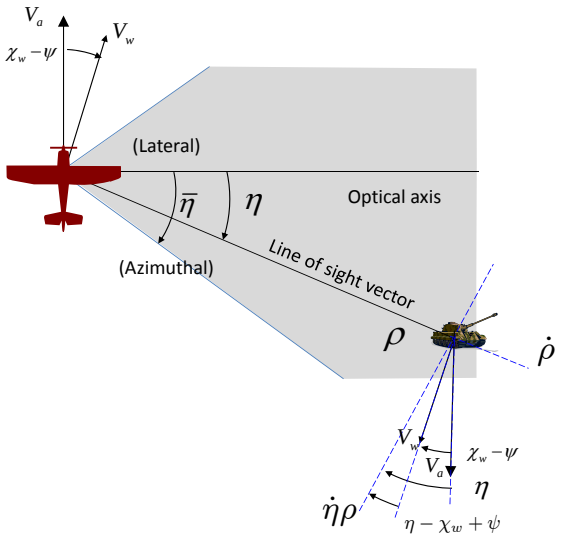

Figure 1: Lateral coordinates of the target as viewed from the MAV body frame.

measured by a right-handed rotation about the body frame z-axis (pointing toward the center of the earth) from the optical axis. The relevant equations of motion are

$$\dot{\rho} = V_a \sin\eta + V_w \sin(\eta - \chi_w + \psi) \tag{1}$$

$$\dot{\eta} = -\frac{g}{V_a}\tan\phi + \frac{V_a}{\rho}\cos\eta + \frac{V_w}{\rho}\cos(\eta - \chi_w + \psi) \tag{2}$$

$$\dot{\psi} = \frac{g}{V_a}\tan\phi, \tag{3}$$

where V_w, V_a, and ψ are the wind speed, airspeed, and heading angles, χ_w is the wind direction, g is the gravitational constant, and ϕ is the commanded roll angle, which is positive when the right wing is down. Throughout the paper we will assume that V_a, V_w, and χ_w are constant.

The MAV is equipped with a camera pointed out of the right wing, at an elevation angle of α_e, allowing it to persistently orbit a target in the camera field-of-view, as shown in Figure 2. The camera is not gimbaled and is fixed in the MAV body frame.

2.2 Camera geometry

The geometry for the lateral field-of-view of the camera is shown in Figure 1. Since the camera is pointed out the right wing, the azimuth angle of the target

in the image is given by the state variable η. Let $\bar{\eta}$ be the limit, due to the field-of-view of the camera, on the azimuth angle. Therefore, to maintain the target in the lateral field-of-view, we require that

$$|\eta| \leq \bar{\eta}.$$

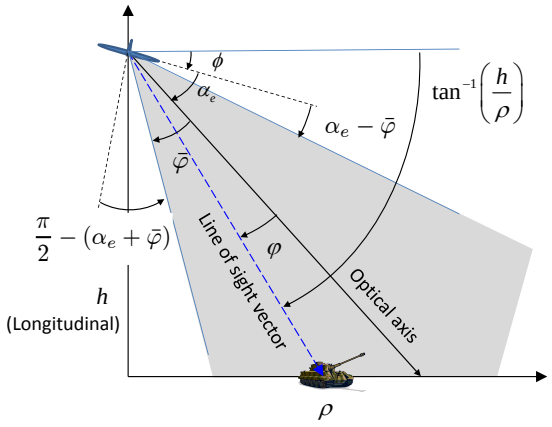

Figure 2: Longitudinal view of camera geometry.

The camera geometry in the longitudinal direction is shown in Figure 2, where ϕ denotes the roll angle of the MAV, α_e is the (constant) elevation angle of the optical axis relative to the body frame, and $\bar{\varphi}$ is the field-of-view limit on the elevation angle. The angular deviation of the line of sight vector from the optical axis is given by

$$\varphi = \tan^{-1}\left(\frac{h}{\rho}\right) - \phi - \alpha_e. \tag{4}$$

To ensure that the target remains in the camera field-of-view, we require that

$$|\varphi| \leq \bar{\varphi}. \tag{5}$$

2.3 Control Objective

The control objective is to minimize the stand-off distance to the target $\rho(t)$ in order to maximize the resolution of the image in the camera frame, subject to the following constraints:

1. $|\eta(t)| \leq \bar{\eta}$ for all $t \geq 0$, where $\bar{\eta}$ is the lateral field-of-view of the camera,
2. $|\varphi(t)| \leq \bar{\varphi}$ for all $t \geq 0$, where $\bar{\varphi}$ is the longitudinal field-of-view of the camera, and
3. $|\phi(t)| \leq \bar{\phi}$ where $\bar{\phi}$ is the maximum allowable roll angle.

We will assume that the constraints are satisfied at time $t = 0$.

3 Target Motion in the Image Plane

3.1 Longitudinal field-of-view

To maintain the target in the longitudinal field-of-view the roll angle must be suitably constrained. In this section we derive the required roll angle constraints and show that they are consistent. With reference to Figure 2 and Equation (4) and (5), the target will remain in the longitudinal field of view if

$$-\bar{\varphi} \leq \tan^{-1}\left(\frac{h}{\rho}\right) - \phi - \alpha_e \leq \bar{\varphi}.$$

Rearranging in terms of the roll angle ϕ we have

$$\tan^{-1}\left(\frac{h}{\rho}\right) - \bar{\varphi} - \alpha_e \leq \phi \leq \tan^{-1}\left(\frac{h}{\rho}\right) + \bar{\varphi} - \alpha_e.$$

Taking into account the physical constraint $|\phi| \leq \bar{\phi}$ we define the roll bounds as

$$\phi_{up} = \min\left(\tan^{-1}\left(\frac{h}{\rho}\right) + \bar{\varphi} - \alpha_e, \bar{\phi}\right), \tag{6}$$

$$\phi_{low} = \max\left(\tan^{-1}\left(\frac{h}{\rho}\right) - \bar{\varphi} - \alpha_e, -\bar{\phi}\right). \tag{7}$$

The idea is that if the roll angle is constrained as $\phi_{low} \leq \phi \leq \phi_{up}$, then the roll angle satisfies $|\phi| \leq \bar{\phi}$, and the target is guaranteed to be in the longitudinal field of view. The following lemma gives conditions for the roll bounds to be consistent.

Lemma 3.1 *If $\bar{\phi}$, $\bar{\varphi}$, and α_e satisfy*

$$\bar{\phi} \geq \max\left\{\frac{\pi}{2} - (\alpha_e + \bar{\varphi}), \alpha_e - \bar{\varphi}\right\}, \tag{8}$$

then $\phi_{low} \leq \phi_{up}$.

In addition, if the roll angle is constrained so that

$$\phi_{low} \leq \phi \leq \phi_{up}, \tag{9}$$

then the target remains in the longitudinal field-of-view.

Proof. To show that $\phi_{low} \leq \phi_{up}$, we need to demonstrate that

Case 1. $\tan^{-1}\left(\frac{h}{\rho}\right) - \bar{\varphi} - \alpha_e \leq \tan^{-1}\left(\frac{h}{\rho}\right) + \bar{\varphi} - \alpha_e$,

Case 2. $\tan^{-1}\left(\frac{h}{\rho}\right) - \bar{\varphi} - \alpha_e \leq \bar{\phi}$,

Case 3. $-\bar{\phi} \leq \tan^{-1}\left(\frac{h}{\rho}\right) + \bar{\varphi} - \alpha_e$,

Case 4. $-\bar{\phi} \leq \bar{\phi}$.

Cases 1 and 4 are trivial. Cases 2 and 3 follows from Equation (8) by noting that $\rho \geq 0$ implies that $0 \leq \tan^{-1}(h/\rho) \leq \pi/2$. ■

Remark 3.1 *As can be seen from Figure 1, the condition in Equation* (8) *ensures that for any position in the sky, there is an allowable roll angle that enables the vehicle to see the target.*

Remark 3.2 *If instead of a strap-down camera, the elevation angle of the camera is controlled by a single axis gimbal, then the target is maintained in the longitudinal field of view by commanding the elevation angle of the gimbal so that φ in Equation* (4) *is equal to zero. The result is*

$$\alpha_e = \tan^{-1}\left(\frac{h}{\rho}\right) - \phi.$$

3.2 Lateral field-of-view

To derive a strategy to maintain the target in the lateral field-of-view, consider the scalar function

$$W = \frac{1}{2}\eta^2, \tag{10}$$

which represents the square of the lateral pointing error. Differentiating W along solutions of (2) gives

$$\dot{W} = \eta\left(-\frac{g}{V_a}\tan\phi + \frac{V_a}{\rho}\cos\eta + \frac{V_w}{\rho}\cos(\eta - \chi_w + \psi)\right). \tag{11}$$

If for the moment we ignore the roll angle constraints, then the roll angle could be selected as

$$\phi^- = \tan^{-1}\left[\frac{V_a}{g}\left(\frac{V_a}{\rho}\cos\eta + \frac{V_w}{\rho}\cos(\eta - \chi_w + \psi) + k\eta - \nu\right)\right], \tag{12}$$

resulting in

$$\begin{aligned}\dot{W} &= -k\eta^2 + \eta\nu \\ &\leq -k\eta^2 + |\eta|\,|\nu| \\ &= -(1-\theta)k\eta^2 + \left[|\eta|\,|\nu| - \theta k\eta^2\right],\end{aligned} \tag{13}$$

where $\theta \in (0,1)$ is a selectable gain. Therefore, $\dot{W}$ is negative definite if $|\nu| < k\theta\,|\eta|$.

Since ϕ^- as given in Equation (12) may not satisfy constraint (9), we propose using the saturated control

$$\phi^c(t) = \begin{cases} \phi_{up} & \text{if } \phi^-(t) \geq \phi_{up} \\ \phi_{low} & \text{if } \phi^-(t) \leq \phi_{low} \\ \phi^-(t) & \text{otherwise} \end{cases}. \tag{14}$$

The next theorem gives sufficient conditions that ensures that when the target begins in the field of view, that it remains in the field of view.

Theorem 3.1 *Suppose that the roll angle is given by Equation* (14) *where* ν *satisfies*

$$|\nu| \leq k\theta\bar{\eta}, \tag{15}$$

for some $\theta \in (0,1)$*, and suppose that Equation* (8) *is satisfied. If*

$$\tan^{-1}\left[\frac{V_a}{g}\left(\frac{V_a\cos\bar{\eta}-V_w}{\rho}-k(1+\theta)\bar{\eta}\right)\right] \geq \max\left\{\tan^{-1}\frac{h}{\rho}-(\bar{\varphi}+\alpha_e), -\bar{\phi}\right\}, \tag{16}$$

for all $\rho > 0$*, then the camera field-of-view is positively invariant, i.e.,* $|\eta(0)| \leq \bar{\eta}$ *and* $|\varphi(0)| \leq \bar{\varphi}$ *imply that* $|\eta(t)| \leq \bar{\eta}$ *and* $|\varphi(t)| \leq \bar{\varphi}$*, for all* $t \geq 0$*.*

Proof. From the definition of ϕ^c in Equation (14) and Lemma 3.1 it follows that if $|\varphi(0)| \leq \bar{\varphi}$, then $|\varphi(t)| \leq \bar{\varphi}$, or in other words, the longitudinal field of view is positively invariant.

To show that the lateral field of view is positively invariant, consider W as in Equation (10). When the roll angle is not saturated then $\phi = \phi^-$, and Equation (13) and constraint (15) implies that both $\dot{W}(\bar{\eta})$ and $\dot{W}(-\bar{\eta})$ are negative. Therefore in the unconstrained case, the set $S_{\bar{\eta}} \stackrel{\triangle}{=} \{-\bar{\eta} \leq \eta \leq \bar{\eta}\}$ is positively invariant. When $\phi^- \leq \phi_{low}$, then $\phi = \phi_{low}$, and Equation (11) becomes

$$\dot{W} = \eta\left(-\frac{g}{V_a}\tan\phi_{low}+\frac{V_a}{\rho}\cos\eta+\frac{V_w}{\rho}\cos(\eta-\chi_w+\psi)\right).$$

Since $\phi_{low} \geq \phi^-$ we have that

$$-\frac{g}{V_a}\tan\phi_{low}+\frac{V_a}{\rho}\cos\eta+\frac{V_w}{\rho}\cos(\eta-\chi_w+\psi) \leq -k\eta+\nu,$$

which implies that $\dot{W} \leq -k\eta^2+\eta\nu$. Therefore, at the lower saturation limit, the set $S_{\bar{\eta}}$ is again positively invariant.

Suppose now that $\phi^- \geq \phi_{up}$ so that $\phi = \phi_{up}$. We need to show that $\dot{\eta}$ is positive when $\eta = -\bar{\eta}$, and negative when $\eta = \bar{\eta}$. When $\eta = -\bar{\eta}$ we have

$$\begin{aligned}\dot{\eta} &= -\frac{g}{V_a}\tan\phi_{up}+\frac{V_a}{\rho}\cos\bar{\eta}+\frac{V_w}{\rho}\cos(-\bar{\eta}-\chi_w+\psi)\\ &\geq k\bar{\eta}+\nu\end{aligned}$$

where the second expression comes from $\phi_{up} \leq \phi^-$. Minimizing the right hand side subject to constraint (15) gives $\dot{\eta} \geq k(1-\theta)\bar{\eta} > 0$.

When $\eta = \bar{\eta}$ we will show that Equation (16) implies that $\phi^- \geq \phi_{low}$ and hence $\dot{\eta} < 0$. Indeed $\phi^-(\bar{\eta}) \geq \phi_{low}(\bar{\eta})$ if and only if

$$\tan^{-1}\left[\frac{V_a}{g}\left(\frac{V_a}{\rho}\cos\bar{\eta} + \frac{V_w}{\rho}\cos(\bar{\eta} - \chi_w + \psi) + k\bar{\eta} - \nu\right)\right] \geq \max\left\{\tan^{-1}\frac{h}{\rho} - (\bar{\varphi} + \alpha_e), -\bar{\phi}\right\}. \quad (17)$$

Minimizing the left hand side over $\chi_w - \psi$ and ν, subject to constraint (15), gives Equation (16). ■

Remark 3.3 *The objective of the control law given in Equation* (14) *is not to drive η to zero, but rather to ensure that η remains in the field of view, i.e., $\eta \in S_{\bar{\eta}}$. Clearly if $\nu(t) = 0$, then η converges to zero. However allowing $\nu \neq 0$ allows an additional degree of freedom that will be exploited in the next section.*

Remark 3.4 *Figure 3 plots the left-hand and right-hand sides of Equation* (16) *for some typical parameters. Assuming that V_a, V_w, $\bar{\eta}$, $\bar{\varphi}$, α_e, and $\bar{\phi}$ are fixed, the designer can adjust the control gain k as well as the altitude h to satisfy Equation* (16)*. We should also note that this constraint is conservative in the sense that we require it to be satisfied for all $\rho > 0$. However, if trajectories of the system can be guaranteed to satisfy $\rho(t) \geq \rho_{\min}$, and Equation* (16) *is only required to hold for $\rho \geq \rho_{\min}$, which as Figure 3 indicates, may be significantly easier to satisfy.*

3.3 Minimizing the range-to-target

The control signal ν in Equation (12) can be selected, subject to constraint (15), to shape the trajectory of the MAV. For example, we may want to maintain the MAV as close as possible to the target, thereby maximizing the resolution of the imagery. Our strategy will be to select ν at time t to minimize a function of ρ, two time steps into the future. Different look-ahead strategies could of course be used. However, since the relative degree from the input ν to the stand-off distance ρ is two, the minimum look-ahead is also two. A two-step look ahead is computationally simple and only requires a one dimensional search, and yet it appears to be an effective strategy as will be shown in Section 4.

Substituting Equation (12) into Equation (2) gives

$$\dot{\eta} = -k\eta + \nu. \quad (18)$$

For the time step T, the sampled-data version of (18) is

$$\eta(t+T) = e^{-kT}\eta(t) + (1 - e^{-kT})\nu(t).$$

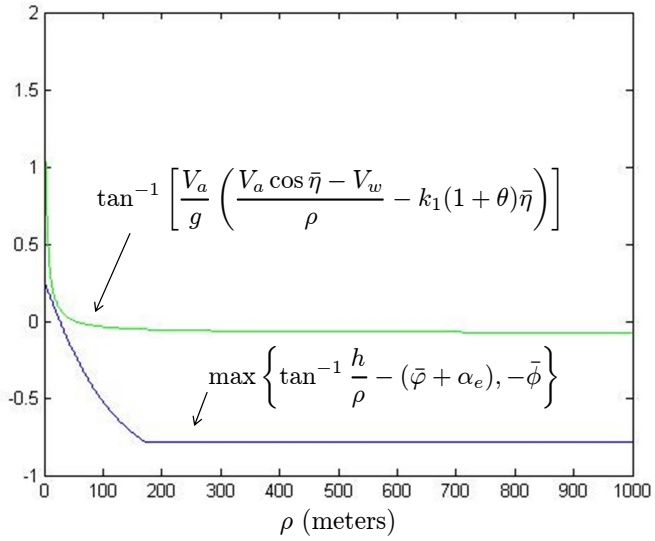

Figure 3: The constraint given by Equation (16) when $V_a = 10\ m/s$, $V_w = 3\ m/s$, $\bar{\eta} = 30$ degrees, $k = 0.05$, $\theta = 0.9$, $h = 100\ m$, $\bar{\varphi} = 30$ degrees, $\alpha_e = 45$ degrees, and $\bar{\phi} = 45$ degrees.

Using an Euler approximation of Equation (1) and (3), where ϕ is given by Equation (12), gives

$$\begin{aligned}
\psi(t+T) &= \psi(t) + T\left[\frac{g}{V_a}\tan\phi(\nu(t))\right] \\
\rho(t+T) &= \rho(t) + T\left[V_a\sin\eta(t) + V_m\sin(\eta(t)-\chi_w+\psi(t))\right] \\
\rho(t+2T) &= \rho(t+T) + T\left[V_a\sin\eta(t+T) + V_m\sin(\eta(t+T)-\chi_w+\psi(t+T))\right]
\end{aligned}$$

Therefore, $\nu(t)$ can be selected as

$$\nu^*(t) = \arg\min_{|\nu(t)|\leq k\theta\bar{\eta}} J(\rho(t+2T)). \tag{19}$$

To minimize the distance to the target we could select $J(\rho) = |\rho|$. To maintain a fixed standoff distance we could select $J(\rho) = |\rho - \rho_{\text{standoff}}|$. Since Euler approximation is poor for large sample time, the time step T should be chosen to be as small as possible. However, if T is chosen to be too small (for example the sample rate of the on-board processor), then there is very little look-ahead over which the control will act. For this paper we used $T = 0.1$ seconds. The minimization in Eq. (19) can be performed using a simple and numerically efficient line search algorithm.

3.4 Resulting Flight Paths

Ref [13] shows that the path of an air vehicle tracking a target in constant wind with a roll only camera is an elliptical orbit if $\eta = 0$. To show that our approach produces a similar result, divide (1) by (3), and use (12) with $\eta = \nu = 0$ to get

$$\frac{d\rho}{d\psi} = \rho \frac{-V_w \sin(\psi - \chi_w)}{V_a + V_w \cos(\psi - \chi_w)}. \tag{20}$$

As pointed out in [9], Equation (20) is an elliptical orbit with eccentricity $\epsilon = \frac{V_w}{V_a}$. One of the advantages of our approach is that rather than forcing the target to be located along the optical axis, the target is allowed (through the selection of ν) to move in the image plane to facilitate more circular orbits in wind. An interesting question is whether circular orbits, where the target remains in the camera field-of-view, are possible in constant wind. The following theorem provides a sufficient condition.

Theorem 3.2 *Circular orbits that maintain the target in the field-of-view are possible if*

$$\tan \bar{\eta} \geq \max_{\psi \in [0, 2\pi]} \left| \frac{-\frac{V_w}{V_a} \sin(\chi_w + \psi)}{1 + \frac{V_w}{V_a} \cos(\chi_w + \psi)} \right|. \tag{21}$$

Proof. Dividing (1) by (3) and using (12) gives

$$\frac{d\rho}{d\psi} = -\rho \frac{V_a \sin\eta + V_w \sin(\eta - \chi_w + \psi)}{V_a \cos\eta + V_w \cos(\eta - \chi_w + \psi) - k\eta + \nu}.$$

When the orbit is circular, $\frac{d\rho}{d\psi} = 0$, or in other words,

$$V_a \sin\eta + V_w \sin(\eta - \chi_w + \psi) = 0.$$

Solving for $\tan\eta$ gives

$$\tan\eta = -\frac{\frac{V_w}{V_a} \sin(\chi_w + \psi)}{1 + \frac{V_w}{V_a} \cos(\chi_w + \psi)}. \tag{22}$$

Maximizing the right hand side of (22) over all possible values of ψ gives Eq. (21). ■

4 Simulation Results

Simulations were conducted in Simulink using a six degree-of-freedom model. We used an emulated Kestrel autopilot [1] with airspeed set to $V_a = 13$ m/s. The location and size of the target in the camera image plane were calculated to emulate vision processing. For all simulation results, the initial position of the MAV is zero meters North, 50 meters East, with heading and roll angles of zero degrees. The target is located at the origin.

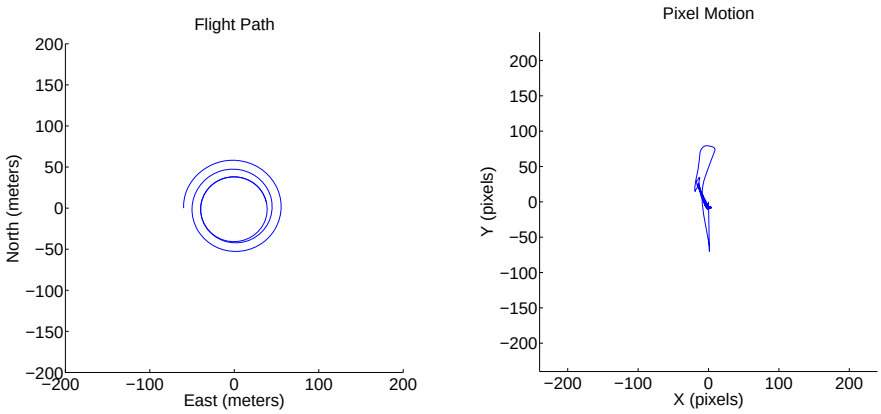

(a) (b)

Figure 4: (a) Simulated flight path using the guidance strategy in Section 3 in zero wind. The MAV's initial configuration allow the camera to capture the target. The MAV navigates onto a stable orbit around the target. The gain is set to $k = 1.5$. (b) The corresponding motion of the target in the image plane.

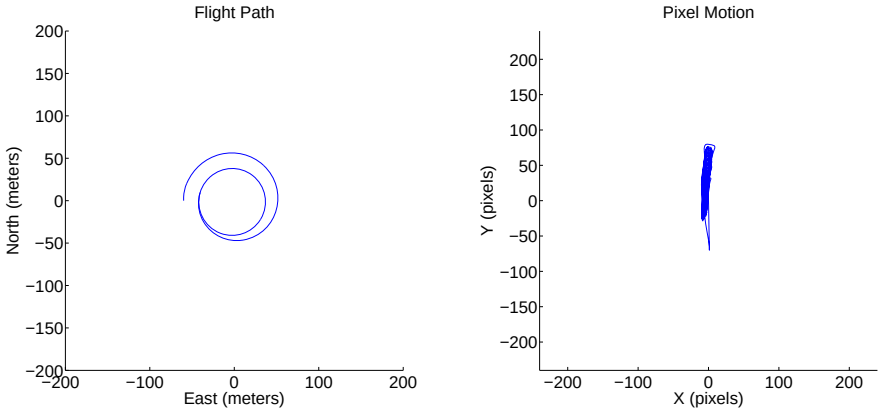

(a) (b)

Figure 5: (a) Simulated flight path in zero wind with gain $k = 5.0$. (b) The corresponding motion of the target in the image plane.

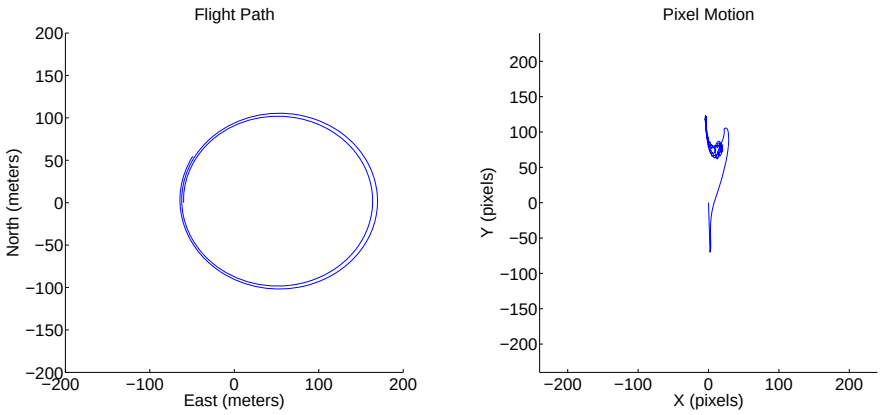

(a) (b)

Figure 6: (a) Simulated flight path result with wind of 5m/s from the North, and parameters set to $k = 5.0$, $\bar{\eta} = 10$ degrees, $\bar{\phi} = 20$ degrees. (b) The corresponding motion of the target in the image plane.

The results of a stationary target in zero wind are shown in Figure 4 (a). Without wind, the expected shape of the orbit is circular. Figure 4 (a) demonstrates the flight path of the MAV converging to a circular orbit as predicted.

The gain k changes the rate of convergence to the orbit. To examine the effect of k on the convergence rates, the gains were set to $k = 1.5$ in Figure 4 (a), and $k = 5.0$ in Figure 5 (a). While a larger gain results in faster convergence, it also induces more target movement in the camera frame. The corresponding target motion in the camera frame are shown in Figures 4 (b), and 5 (b).

The results of a stationary target in a constant wind of $V_w = 5$ m/s to the North are shown in Figure 6 (a). Notice that the flight path converges to an ellipse as was predicted in [13], without explicit path planning. The corresponding motion of the target in the image plane is shown in Figure 6 (b).

The constraint $\bar{\eta}$ bounds the movement of the target in the camera field-of-view. If the bound is relaxed, the target can move more in the camera field-of-view. The result is a more circular orbit, or an ellipse with a lower eccentricity. Figures 6 (a) and 7 (a) show the flight path for $\bar{\eta} = 10$ degrees and $\bar{\eta} = 30$ degrees, respectively. The eccentricity of the ellipse decreases from 0.42 for $\bar{\eta} = 10$ degrees to 0.33 for $\bar{\eta} = 30$ degrees. In addition, the target motion in the camera field-of-view increases as shown in Figures 6 (b) and 7 (b).

The results of a stationary target in a constant wind of $V_w = 7$ m/s to the East with gusts that are Gaussian with standard deviation of $\sigma = \sqrt{30}$ m/s are shown in Figure 8 (a), with corresponding pixel motion shown in Figure 8 (b). Note that although the pixel motion is more jumpy, the algorithm maintains the target in the camera field-of-view showing the robustness of the algorithm to fairly strong wind gusts.

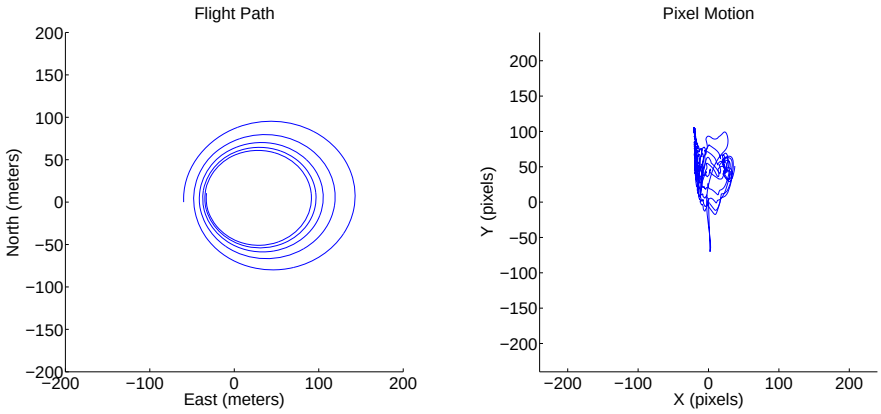

(a) (b)

Figure 7: (a) Simulated flight path result with wind of 5m/s from the North, and parameters set to $k = 5.0$, $\bar{\eta} = 30$, $\bar{\phi} = 20$ degrees. (b) The corresponding motion of the target in the image plane.

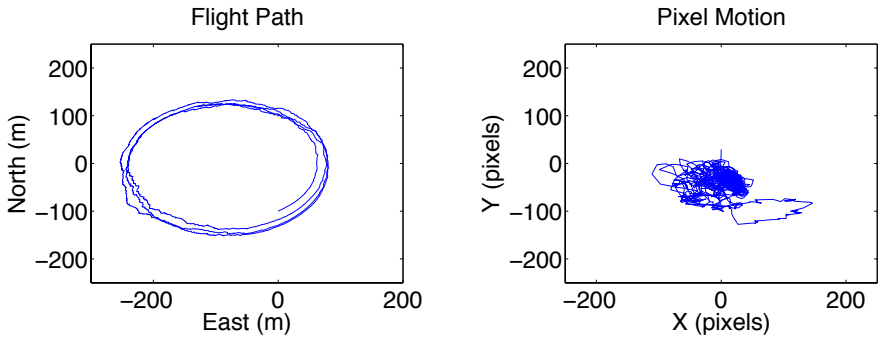

(a) (b)

Figure 8: (a) Simulated flight path with constant wind of 7 m/s from the East, and random wind gust with variance $\sigma = \sqrt{30}$. (b) The corresponding motion of the target in the image plane.

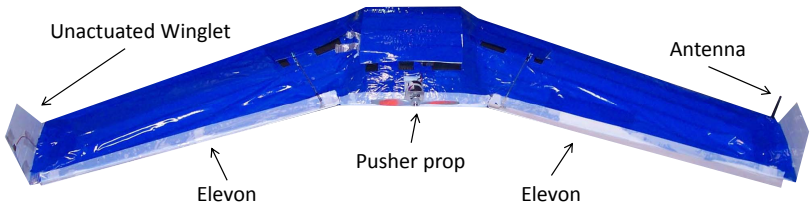

Figure 9: The MAV has a wing span of approximately 48 inches and uses the Kestrel autopilot from Procerus Technologies.

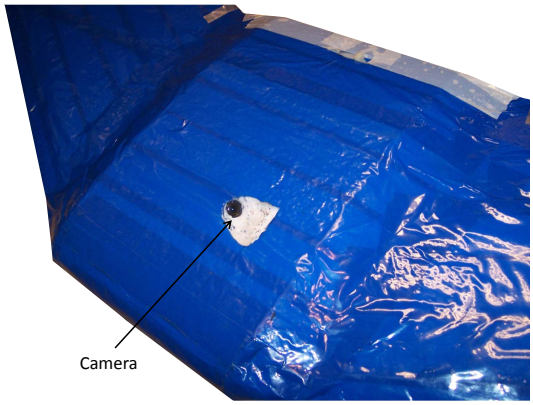

Figure 10: The camera is mounted under the MAV at an elevation angle of 30 degrees.

5 Flight Results

Flight tests were conducted using a MAV with a 48 inch wing span, a pusher propeller with two elevon control surfaces as shown in Figure 9, and the Kestrel autopilot from Procerus Technologies [1]. For the camera, we used a Panasonic KX-141 with 480 lines of resolution mounted on the MAV at an azimuth angle of 90 degrees (out the right wing) and an elevation angle of $\alpha_e = 30$ degrees, as shown in Figure 10. The wind speed during the flight tests was approximately 2 m/s. The parameters were $k = 3$, $\bar{\eta} = 10$ degrees, and $\bar{\phi} = 15$ degrees.

The video was transmitted to the ground station via a 2.4 GHz analog transmitter, where a color segmentation algorithm was used to locate the target in the image frame. The target was a red cloth on the ground. The color segmentation algorithm used thresholds to remove all colors other than red, and

Figure 11: The ground station processes video by color segmentation to find the location of the red cloth.

returned the location of the largest patch of red. A representative image from the video sequence is shown in Figure 11. The color segmentation algorithm runs at 30 frames per second with a delay of approximately 0.5 seconds. The control algorithm is implemented on the ground station and transmitted via a 900 MHz transceiver to the aircraft.

The resulting flight path of the MAV, and the corresponding target motion in the camera field-of-view is shown in Figure 12. The ambient wind resulted in an elliptical orbit with eccentricity $\epsilon = 0.17$. The theoretical prediction for a wind of $V_w = 2m/s$ is $\epsilon = \frac{V_w}{V_a} = 0.15$. The guidance algorithm presented in this paper successfully maintained the target in the field-of-view of the camera throughout the flight test. We note that since we were flying in the atmosphere that the MAV was subject to occasional wind gusts. The flight tests results indicate a level of robustness to these gusts.

6 Conclusion

This paper has considered the problem of tracking a target using a strap-down camera on a small unmanned air vehicle. The novel idea presented in this paper is that the target can be pushed around in the image plane by maneuvering the vehicle. In particular, if the low level autopilot induces bank-to-turn dynamics (by regulating side-slip to zero), then the roll angle induces yaw and can be used to "push" the projection of the target in the image plane. We have derived explicit constraints on the roll angle to ensure that the target does not leave the camera field-of-view, and have allowed an additional degree of freedom that can be exploited to control the stand-off distance. We have also shown that in the absence of wind, the flight path that results from this guidance law is an optimal elliptical orbit. We have shown conditions on the wind that allow

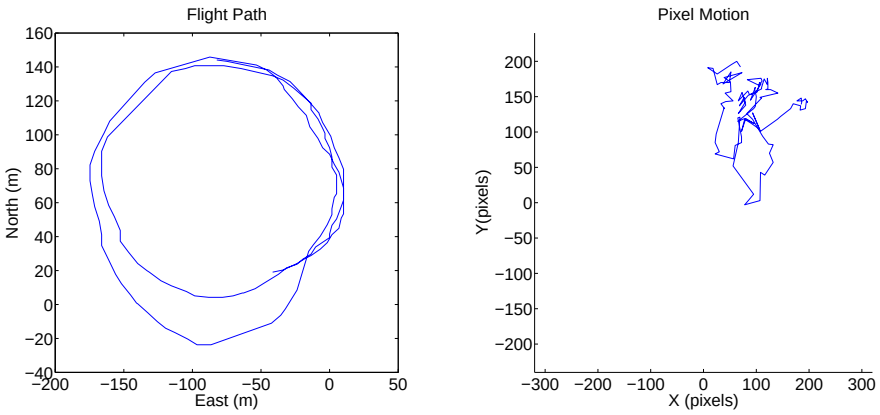

(a) (b)

Figure 12: (a) Flight results using the algorithm described in Section 3 in constant ambient wind of approximately $V_w = 2m/s$. (b) The corresponding motion of the target in the image plane.

the target to remain in the field of view when the aircraft is flying a circular orbit. Simulation and flight results verify the effectiveness of the approach. Both simulations and flight tests demonstrate the effectiveness of the algorithm and its robustness with respect to wind gusts, although the level of robustness has not been quantified analytically.

Acknowledgement

This research was funded in part by the Air Force Research Laboratory, Munitions Directorate under SBIR contract No. FA 8651-07-C-0094 to Scientific Systems Company, Inc. and Brigham Young University and by NSF award No. CCF-0428004. Portions of this work were accomplished while the first author participated in the Air Force Research Laboratory's Summer Research Program at Wright-Patterson AFB.

References

[1] Procerus Technologies. `http://procerusuav.com/`.

[2] E.W. Frew, X. Xiao, S. Spry, T. McGee, Z. Kim, J. Tisdale, R. Sengupta, and J. K. Hendrick. Flight demonstrations of self-directed collaborative navigation of small unmanned aircraft. In *AIAA 3rd Unmanned Unlimited Technical Conference*, September 2004.

[3] Ruggero Frezza and Claudio Altafini. Autonomous landing by computer vision: an application of path following in SE(3). In *Conference on Decision and Control*, December 2004.

[4] Jusuk Lee, Rosemary Huang, Andrew Vaughn, Xiao Xiao, and J. Karl Hedrick. Strategies of path-planning for a UAV to track a ground vehicle. In *Proceedings of the 2nd Anual Autonomous Intelligent Networks and Systems Conference*, 2003.

[5] L. Ma, C. Cao, V. Dobrokhodov, I. Kaminer, K. Jones, and I. Kitsios. Rapid motion estimation of a target moving with time-varying velocity. In *AIAA Guidance, Navigation and Control Conference and Exhibit*, August 2007.

[6] L. Ma, C. Cao, N. Hovakimyan, C. Woolsey, V. Dobrokhodov, and I. Kaminer. Development of a vision-based guidance law for tracking a moving target. In *AIAA Guidance, Navigation and Control Conference and Exhibit*, August 2007.

[7] Ruggero Rezza. Path following for air vehicles in coordinated flight. In *International Conference on Advanced Intelligent Mechatronics*, September 1999.

[8] Rolf Rysdyk. Unmanned aerial vehicle path following for target observation in wind. *Journal of Guidance, Control, and Dynamics*, 29(5):1092–1100, September-October 2006.

[9] Rolf Rysdyk. Unmanned aerial vehicle path following for target observation in wind. *Journal of Guidance, Control, and Dynamics*, 29(5):1092–1100, September-October 2006.

[10] Bruno Sinopoli, Mario Micheli, Gianluca Donatot, and T. John Koo. Vision based navigation for an unmanned aerial vehicle. *Proceedings of the 2001 IEEE International Conference on Robotics and Automation*, pages 1757–1764, 2001.

[11] Vahram Stepanyan and Naira Hovakimyan. Visual tracking of a maneuvering target. In *AIAA Guidance, Navigation and Control Conference and Exhibit*, August 2006.

[12] S. Stolle and R. Rysdyk. Flight path following guidance for unmanned air vehicles with pan-tilt camera for target observation. In *Digital Avionics Systems Conference*, 2003.

[13] P.G. Thomasson. Guidance of a roll-only camera for ground observation in wind. *Journal of Guidance, Control, and Dynamics*, 21(1):39–44, January-Feburary 1998.

[14] Ick H. Wang, Vladimir N. Dobrokhodov, Isaac I. Kaminer, and Kevin D. Jones. On vision-based target tracking and range estimation for small UAVs. In *AIAA Guidance, Navigation and Control Conference and Exhibit*, August 2005.

[15] Huili Yu, Rajnikant Sharma, and Randal W. Beard. Observability-based local path planning and collision avoidance for micro air vehicles using bearing-only measurements. In *Proceedings of the American Control Conference*, page (in review), 2011.